Version 29/09/201511:09:36

Petrology of a non-indigenous microgranitic clast in polymict ureilite EET 87720: evidence for formation of evolved melt on an unknown parent body.

Beard, A.D.[1]*, Downes, H.[1,2] and Chaussidon M.[3]

1. UCL/Birkbeck Centre for Planetary Sciences, and Department of Earth and Planetary Sciences, Birkbeck, Malet Street, London, WC1E 7HX, UK.
2. Department of Earth Sciences, Natural History Museum, Cromwell Rd, London, UK
3. Institute of Physics of the Globe, 1 Rue Jussieu, Paris, France

*Corresponding author. a.beard@ucl.ac.uk

Abstract

EET 87720 is a polymict ureilite breccia known to contain numerous non-indigenous fragments. We have discovered a microgranitic clast in an interior chip of EET 87720. The clast consists of a granophyre-like intergrowth of a pure SiO_2 phase (tridymite) and albite, mantling a zoned oligoclase phenocryst. In the intergrowth, the tridymite occurs as thin elongate vermicular blebs within larger albite crystals. The granophyre-like intergrowth and the oligoclase phenocryst share a common margin, suggesting that the clast was originally part of a larger fragment. An estimate of its bulk composition is equivalent to that of granite (77 wt.% SiO_2). Patches of high-Si K-bearing glass occur interstitially within the clast; they have high concentrations of SO_3 (11-12 wt.%) and contain Cl (0.6 wt.%), suggesting that the clast formed on a volatile-rich parent body perhaps resembling early Mars. The mean oxygen isotope composition of the feldspar and tridymite in the clast is very different from the oxygen isotope compositions of ureilites, and is similar to those of silicate inclusions in IIE and IVA irons. Thus the clast is not indigenous to the ureilite parent body, but it provides evidence for the formation of evolved melts on an unknown parent body in the early solar system.

Introduction

A fundamental question in studies of the early Solar System is whether the process that formed granitic rocks on the early Earth (Guitreau et al., 2012) also occurred on other terrestrial planets or differentiated planetesimals. Bonin (2012) reviewed the occurrences of "extra-terrestrial granites" and suggested that such granites are more common than had previously been thought. Granitic clasts have been found in the Adzhi-Bogdo LL3-6 chondrite meteorite (Bischoff et al., 1993) and the Buzzard Coulee chondrite (Ruzicka et al. 2012). Pb-Pb dating of the Adzhi-Bogdo clasts suggests that granitic melts forms on a primitive asteroid 4.53 Ga ago (Terada and Bischoff, 2009), within a few Ma of the formation of CAIs. These "grandparent" primitive asteroids along with their granitic igneous bodies were subsequently fragmented by impact, mixed and reaccreted as the brecciated Adzhi-Bogdo meteorite parent body ago (Terada and Bischoff, 2009). Day et al. (2009) also reported the occurrence of quartz-normative andesitic meteorites (GRA 06128/9) with an age of 4.517 Ga. Felsic or siliceous inclusions are also known from IIE irons and the ungrouped iron Sombrerete (Ruzicka et al. 2006; Ruzicka and Hutson 2010; Ruzicka 2014). We report here mineral chemical and oxygen isotopic data for a microgranitic clast within a polymict ureilite meteorite, which adds to the evidence for the formation of evolved magmas on early solar system bodies.

Ureilites are the second largest group of achondritic meteorites (Mittlefehldt et al., 1998; Goodrich et al., 2004). Most ureilites are unbrecciated ultramafic rocks consisting of olivine and pyroxene, representing the mantle of the ureilite parent body (UPB). However, several are polymict breccias, considered to represent the regolith formed on or near to the surface of the UPB (Warren and Kallemeyn, 1989; Goodrich et al., 2004). Polymict ureilites contain a large variety of clasts, some of which are clearly ureilitic, but others are different from common ureilitic material and must have been derived from other solar system bodies (Goodrich et al., 2004; Kita et al., 2004; Bischoff et al., 2006; Downes et al., 2008). The fall of Almahata Sitta (Horstmann and Bischoff, 2014; Goodrich et al., 2014) has yielded new insights into the nature of the UPB, as approximately 20-30% of the recovered mass of this meteorite was non-ureilitic. Bischoff

et al (2014) have reported the discovery of a trachyandesitic meteorite with ureilitic affinities among the recovered Almahata Sitta stones. In this study, we extend the variety of clasts found in polymict ureilites with the discovery of an igneous-textured granitic clast in an Antarctic polymict ureilite Elephant Moraine (EET) 87720.

Samples and analytical techniques

The sample investigated in this study is a polished thick-section prepared from an interior chip of EET 87720. The section (,41) was previously studied by Downes et al. (2008). EET 87720 is a cataclastic aggregate (Fig. 1) dominated by clasts of olivine, up to 3mm in diameter, plagioclase and minor amounts of low-Ca pyroxene with traces of Ni-rich iron, troilite, suessite and graphite, set in a clast-supported matrix of finer mineral clasts. It is petrologically similar to other polymict ureilites such as EET 83309, North Haig and Nilpena (Prinz et al., 1987; Downes et al., 2008). Detailed electron microprobe and ion microprobe analyses on the clast population have been reported in several previous studies (Guan and Crozaz, 2000, 2001; Cohen et al., 2004; Kita et al., 2004; Downes et al., 2008). EET 87720 contains solar-implanted gases indicating a regolith origin (Rai et al., 2003).

Major element mineral analyses were obtained using a Jeol JXA8100 Superprobe (WDS) at Birkbeck. Analysis was carried out using an accelerating voltage of 15 kV, current of 25nA and a beam diameter of 1 μm. The counting times for all elements were 40 seconds on the peak and 20 seconds each on the high and low backgrounds. However, counting times for Na and K for the glass were reduced to 20 seconds on the peak and 10 seconds for the background to reduce possible volatile loss. The analyses were calibrated against standards of natural silicates, oxides and Specpure® metals with the data corrected using a ZAF program. Electron microprobe data for mineral phases and glass in the microgranitic clast are given in Table 1, and its modal mineral abundance (%) is given in Table 2, compared with other known meteoritic and lunar granitic clasts.

Because of its small size, the bulk elemental composition of the microgranitic clast could not be directly analysed. However, it was possible to obtain its bulk element composition by multiplying the average compositions of the mineral phases (Table 1) by the modal fraction of the phases (Table 2). The mineral modal fraction was obtained by calculating the proportion of minerals within each $1cm^2$ grid, superimposed on enlarged elemental distribution maps of the clast. The resulting bulk elemental composition is shown in Table 3. The bulk data were then used to determine the normative mineralogy via a CIPW normalisation program (Table 3). The normative mineralogy was then used to classify the rock type using the QAP diagram of Streckeisen (1976).

Spatially-resolved, non-destructive X-ray microdiffraction was performed on the silica phase in the microgranite clast in EET87720,41 using a Rigaku D/MAX-RAPID II X-ray diffractometer at the Natural History Museum, London, UK. The diffractometer was configured with a semicylindrical image-plate detector around a 2-axis sample goniometer, upon which the thin section was mounted. The Cu K alpha beam was collimated and restricted to a diameter of 30 µm by an exit pin hole, and with the sample oriented at an angle of 20 degrees to the incident X-ray beam the footprint of the beam on the sample was approximately 100 µm (e.g. Lambiv-Dzemua et al., 2013). The sample was continually rotating throughout the 19 hour data collection. Phase identification was performed with the aid of the ICDD PDF-2 Powder Diffraction File database.

Oxygen isotope compositions were obtained from albite and silica phases in the microgranite clast at CRPG-CNRS (Nancy, France) using a multi-collector Cameca ims 1280HR2 ion microprobe. The analyses were made using procedures previously described (Chaussidon et al., 2008) using a primary Cs beam of ≈ 0.5 nA intensity and 30 µm diameter and electron gun for charge compensation. The $^{16}O^-$, $^{17}O^-$ and $^{18}O^-$ ion beams were measured on three collectors (the off axis L'2 Faraday cup, the central electron multiplier EM and the off axis H2 electron multiplier, respectively) at a mass resolution $M/\Delta M$ of 2500 for $^{16}O^-$ and $^{18}O^-$ ion and of ≈6000 for $^{17}O^-$. Dead times of 44 and 68 nsec were determined and used for correction of data acquired on the two electron multipliers, EM and H2 respectively. A set of four "in house" standards (quartz, olivine,

magnetite, calcite) were used to determine the instrumental fractionation law of the three oxygen isotopes, which was then used to correct data acquired on the minerals of the microgranitic clast. The measurements were corrected for matrix effect, taking into account that the spots analysed are mainly on feldspar, using the instrumental fractionation determined on the quartz standard, and the law previously determined which shows that matrix effects are primarily dependent on the SiO_2 content of the silicate mineral analyzed (Chaussidon et al., 2008).

The oxygen isotopic compositions are expressed in the classical delta notation in permil relative to the SMOW international standard ($\delta^{17,18}O_{sample}$= 1000 x [($^{17,18}O/^{16}O)_{sample}/(^{17,18}O/^{16}O)_{standard}$ -1]. The two sigma errors given in Table 4 for $\delta^{17,18}O$ values are the quadratic sum of the errors due to counting statistics (≈±0.35‰ and ±0.15‰ for $\delta^{17}O$ and $\delta^{18}O$, respectively), the external reproducibility (two sigma error) on the quartz standard, and the 2 sigma error due to the correction for matrix effect. The ^{16}O excesses are expressed as $\Delta^{17}O$ values with $\Delta^{17}O=\delta^{17}O-0.52x\delta^{18}O$. The two sigma errors given for the $\Delta^{17}O$ values in Table 4 are calculated by summing in quadratic mode the errors due to counting statistic on the $\delta^{17,18}O$ values (before correction for instrumental fractionation) with the external reproducibility (two sigma errors) on the four terrestrial standards analyzed (19 measurements) giving $\Delta^{17}O = 0 \pm 0.11$‰ (two sigma error).

Petrology and mineral chemistry of the microgranitic clast in EET 87720

The microgranitic clast in EET 87720,41 is approximately 550 x 850 μm in size (0.47 mm^2) and consists largely of albite and oligoclase together with a pure silica phase which has been tentatively identified by micro-XRD as tridymite. Tridymite and other silica polymorphs have been previously reported in igneous-textured clasts in the Parnallee (LL3) chondrite (Bridges et al., 1995), and identified in Martian meteorite NWA 856 (Leroux and Cordier 2006) and the LaPaz Icefield lunar basaltic meteorites (Righter et

al., 2005). Figure 2 shows element distribution maps of the entire clast, emphasizing the texture and mineral variation, together with an interpretative schematic of the clast mineralogy. Oligoclase occurs as the core of a single large (150 x 225 μm) euhedral phenocryst, which is strongly zoned to an albitic rim. The tridymite and albite occur as a granophyre-like intergrowth, covering an area of 150x200 μm and mantling the oligoclase crystal. In the intergrowth, the tridymite occurs as thin elongate vermicular blebs, with an average diameter of 5-10 μm and up to 100-120 μm in length within larger albite crystals. Outside the intergrowth, the tridymite and albite also occur as anhedral crystals up to 150 μm in diameter along with two anhedral areas of glass, up to 100 μm in diameter (Fig. 2). Although the normal granophyre mineralogy of K-feldspar and quartz does not occur within this clast, the texture is very similar to that of terrestrial granophyres. The granophyre-like intergrowth and the oligoclase crystal share a common margin, suggesting that the microgranitic clast was originally part of a larger fragment**.**

Albite within the granophyre-like intergrowth has a slightly variable composition (Ab_{91-94}) with a low K_2O content (~1 wt. %) and traces of FeO (0.1-0.3 wt. %). The tridymite in the intergrowth is slightly impure, containing up to 1.3 wt. % Al_2O_3, 0.11 wt. % FeO and 0.2 wt. % Na_2O, similar to quartz in granitic clasts found in the Adzhi-Bogdo LL3-6 chondrite (Bischoff et al., 1993). The phenocryst is strongly zoned from oligoclase (An_{12}) in its core to an albitic rim ($An_{0.05}Ab_{99}Or_{0.7}$). On an Ab-An-Or ternary diagram (Fig. 3), the albite and oligoclase have compositions similar to those found in felsic clasts from polymict ureilite DaG 319 (Ikeda et al, 2000; Ikeda and Prinz, 2001) and albite in the granitic clasts in Adzhi-Bogdo (Bischoff et al., 1993). K-feldspar and more anorthitic plagioclase from small lunar granite samples from the Apollo 14 landing site (Ryder, 1976; Warren et al., 1983; Jolliff et al., 1990) are also plotted for comparison.

Glass occurs as two small patches within the microgranite clast. Even under high magnification in backscattered images, it appears completely devoid of crystallites. As the glass and the tridymite/albite intergrowth share a common broken margin, the glass is clearly part of the clast and has not been introduced from outside. It may therefore be a

melt residue that was quenched after crystallisation of the minerals within the granophyre-like intergrowth. It contains up to 72 wt.% SiO_2, 9.7 wt.% Al_2O_3, 3 wt.% MgO and 1.2 wt.% K_2O. It has an extremely unusual volatile composition with a very high SO_3 content (11-12 wt.%) and 0.6 wt.% Cl (Table 1).

The bulk composition of the microgranite clast, calculated from modal abundance and mineral compositions, plot in the granite field of the TAS diagram (Fig. 4), as used by Bonin (2012) for extraterrestrial granites. It plots in a similar region as the bulk compositions of several glassy inclusions from IIE irons (Takeda et al., 2003). Its Na_2O content greatly exceeds its K_2O content, as is common in silicate glass inclusions in iron meteorites (Bonin 2012) but differs from the Adzhi-Bogdo granitic clasts. The composition of granitic material found within a Martian gabbro (Gross and Filiberto 2014a,b) also shown plots near the mean composition of the microgranite clast from EET 87702,41.

The normative composition of the clast plots in the alkali granite field of the QAP diagram (Fig. 5). The calculated CIPW normative mineralogy for granitic clasts in Adzhi-Bogdo (Bischoff et al., 1993), silica-rich glass inclusions in polymict ureilite DaG 319 (Ikeda and Prinz, 2001; Ikeda et al., 2000), silica-rich glass inclusions in the Colomera IIE iron (Takeda et al., 2003), lunar granites (Warren et al., 1983; Ryder, 1976), felsic glass spherule in howardite NWA 1664 (Barrat et al., 2009) and selected silica-rich glass inclusions in olivine from Martian meteorites DaG 489 (Folco et al., 2000) and Chassigny (Varela et al., 2000) have been plotted on the QAP diagram for comparison (Fig. 5). The majority of granitic clasts from Adzhi-Bogdo and glass inclusions from DaG 319 and Colomera IIE iron, plot in a confined range from alkali syenite to alkali granite. Lunar granite samples have a wider range, plotting within the alkali granite and syenogranite fields. A glass inclusion from the Martian meteorite Chassigny plots in the syenogranite field, while glass inclusions from shergottite DaG 489 plot in the monzogranite and quartz granite fields. The felsic glass spherule in howardite NWA 1664 plots in the monzogranite field.

Oxygen isotope analysis

The data obtained for ten spots made on the feldspar and tridymite within the microgranitic clast in EET 87720,41 are shown in Table 4. Mean values with their two sigma standard deviation errors are: $\delta^{18}O = 3.26 \pm 1.34‰$, $\delta^{17}O = 2.36 \pm 0.88‰$, and $\Delta^{17}O = 0.66 \pm 0.52‰$. The relatively large errors on the $\delta^{17,18}O$ values are likely due to the low secondary ion intensity (required for a small size of the beam) and to small variations of matrix effects which cannot be totally corrected for. On a three isotopes diagram (Fig. 6), the present data plot within error on the YR line of slope 1 (Young and Russell, 1998), significantly above the terrestrial fractionation line, far from the region of ureilites, and close to the field of H chondrites and of silicate inclusions in IIE irons (Clayton and Mayeda, 1996). The microgranitic clast has, within error, the same $\Delta^{17}O$ as a similar object previously found in the LL3-6 Adzhi-Bogdo ordinary chondrite ($\Delta^{17}O = 0.95 \pm 0.27\%$ but with a ≈3.5‰ higher $\delta^{18}O$ value, Sokol et al., 2007). Two other similar clasts from Sokol et al. (2007) have much higher $\Delta^{17}O$ values (+1.79±0.16‰ and +1.93±0.19‰, respectively) and cannot derive from the same differentiated parent body as the clast in EET 87720,41. The data plot marginally above the fractionation line for Martian (SNC) meteorites (Clayton and Mayeda, 1996) and on an extension of the fractionation line for Mars meteorites NWA 7034 (Agee et al., 2013) and NWA 7475 (Wittmann et al., 2015).

Discussion

It is well known that the regolith of the ureilite parent body contains non-indigenous clasts derived from a number of different parent bodies which were transported to the surface of the ureilite parent body as meteorites (Goodrich et al., 2004; Kita et al., 2004). A petrological study of clasts in polymict ureilite (DaG 319) by Ikeda et al. (2000) resulted in a classification scheme consisting of 7 major groups with 24 types of lithic fragments and 22 types of mineral fragments. It is not therefore surprising that new

varieties of clast are still being identified (e.g. Downes et al., 2008; Goodrich and Gross, 2015). However, few of the previously described clasts could be easily related to the microgranitic clast described here, although Ikeda et al. (2000) reported that the mesostasis in a felsic clast in DaG 319 was a mixture of feldspar and silica.

Igneous-textured granitic clasts are relatively rare among granitic material in meteorites (Sokol et al., 2009) and returned lunar samples (Warren et al., 1983; Kuehner et al., 2007), although granitic material showing graphic intergrowths has recently been reported from within a gabbroic Martian meteorite (Gross and Filiberto, 2014a,b). Granophyric intergrowths in terrestrial rocks consist of branching/radiating quartz in a larger single K-feldspar grain, often occurring as a mantle around a pre-existing subhedral-euhedral plagioclase grain. A graphic intergrowth consists of subhedral skeletal quartz crystals in a K-feldspar or sodic plagioclase crystal. The quartz crystals usually have a regular geometric orientation that resembles "cuneiform" writing. All of the different types of granitic intergrowths are indicative of rapid cooling and the simultaneous crystallisation of quartz, K-feldspar and/or plagioclase. In EET 87720, the microgranitic clast consists of an intergrowth of branching tridymite crystals in a larger albite grain, and occurs as mantle around a much larger zoned subhedral oligoclase phenocryst. Although the host feldspar is albite rather than K-feldspar, the general texture is more typical of a granophyre intergrowth rather than myrmekitic or graphic intergrowths.

On Earth, approximately 86 vol% of the upper continental crust is granitic in composition or origin (Wedepohl, 1991), with smaller volumes of granitic rocks in the lower continental crust (charnockites), oceanic crust (plagiogranites) and upper mantle (Bonin and Bébien, 2005). No other body in the solar system is thought to have such an evolved crust, although andesitic and trachyandesitic meteorites have recently been reported (Day et al. 2009; Bischoff et al. 2014) that are expanding the range of magma compositions that erupted on asteroidal surfaces. Other reports of granitic rocks with an extra-terrestrial origin include granitic rock fragments within breccias and soil samples returned from several Apollo landing sites (Rutherford et al., 1976; Ryder, 1976; Warren, 1983;

Martinez and Ryder, 1989; Morris et al., 1990), granitic clasts in the Adzhi-Bogdo LL3-6 chondrite (Bischoff et al., 1993), a granitic clast displaying a micrographic texture in gabbroic shergottite (NWA 6963) (Gross and Filiberto, 2014) and granophyric clasts in lunar meteorite NWA 4472 and NWA 4485 (Kuehner et al., 2007). Barrat et al. (2009) proposed that evolved magmas may also have occurred on the asteroid 4 Vesta because of the presence of glass impact spherules with granitic compositions from several howardite meteorites.

Formation of granitic magma on Earth can occur by anatexis of pre-existing silica-rich feldspar-bearing material, by extensive fractionation of basaltic magma, or by partial melting of pre-existing igneous rocks. The latter two mechanisms do not require any continental crustal or sedimentary material to be present. For lunar granite petrogenesis various models have been considered, including fractional crystallisation producing acidic residual melts (Ryder, 1976) and fractional crystallisation of a basaltic melt followed by silicate liquid immiscibility (Rutherford et al., 1976; Jolliff et al., 1990). Hagerty et al. (2006) proposed an additional model whereby basaltic underplating of the lunar crust resulted in its partial melting and the generation of small-scale granite intrusions. The recently discovered granitic compositions on Mars have been ascribed to extreme fractional crystallization of a basaltic magma (Gross and Filiberto, 2014a,b). Usui et al (2015) studied low pressure experimental partial melting of a H chondrite analogue which showed that siliceous (quartz-normative) melts can be formed by very small degrees of melting under reducing conditions. Experimental studies by Gardner-Vandy (2014) confirm that evolved melts can be formed on an asteroid-sized body through low-degree melting of an oxidized, volatatile-rich chondritic precursor. Terada and Bischoff (2009) suggested that the granitic clasts in the Adzhi-Bogdo meteorite were formed by fractional crystallization or liquid immiscibility from large-scale melting produced the granitic melt. Our data are not sufficient to distinguish between these alternatives for the origin of the micrograniticclast in EET 87720.

The high-Si glass inside the microgranite clast has an extremely unusual composition with 11-12 wt.% SO_3 and some Cl. None of the other granitic or high-Si meteoritic clasts reported in the literature contain these high amounts of volatiles. The high S- and Cl-contents indicate a volatile-rich parent body, which is unlikely to be the parent body of ureilite meteorites which are known to be depleted in volatile elements. The only extant planetary body known to contain abundant SO_3 and Cl is Mars (Leshin et al. 2013), which is thought to have experienced a major impact event early in its history (Marinova et al., 2008). The oxygen isotope composition of the microgranite clast is close to those of Martian meteorites (Fig. 6), and lies on an extension of the $\Delta^{17}O$ = +0.6‰ fractionation trend for Mars breccia meteorites (Agee et al., 2013; Wittmann et al., 2015). Thus although the identity of the parent body of the microgranite clast remains unresolved, some of the evidence points towards Mars.

Conclusions

This study has shown that the microgranitic clast in ureilite EET 87720 was derived from a S- and Cl-rich parent body, with a $\Delta^{17}O$ value of +0.66 ‰, similar to that of Mars breccias NWA 7034/7475 and some of the silicate inclusions in IIE and IVAB iron meteorites. The clast provides further evidence for formation of evolved melt by either extreme fractional crystallization, liquid immiscibility or very low degrees of partial melting on terrestrial parent bodies in the early solar system. The parent body was subsequently impacted or fragmented and a small fragment of it accreted onto the ureilite parent body.

Acknowledgements

We thank the Meteorite Working Group for providing the sample, and Caroline Smith (Natural History Museum, London), Katie Joy (University of Manchester) and Nachiketa Rai (NHM/Birkbeck) for discussions about the origin of this clast. Reviews by B Cohen, K Gardner-Vandy, J Gross, A Ruzicka and Associate Editor Cyrena Goodrich greatly

improved the final version of this paper. Thanks for Paul Schofield and Jens Najorka (NHM) for identifying the tridymite by micro-XRD.

References

Agee C. B. and 15 co-authors,. 2013. Unique meteorite from early Amazonian Mars: Water-rich basaltic breccia Northwest Africa 7034. Science 339, 780-785.

Barrat J.A., Bohn M., Gillet PH. and Yamagichi A. 2009. Evidence for K-rich terranes on Vesta from impact spherules. Meteoritics and Planetary Science 44, 359-374.

Bischoff A., Geiger T., Palme H., Spettel B., Schultz L., Schlûter J. and Lkhamsuren J. 1993. Mineralogy, chemistry and noble gas contents of Adzhi-Bogdo - an LL3-6 chondritic breccia with L-chondritic and granitoidal clasts. Meteoritics 28, 570-578.

Bischoff A, Scott E D, Metzler K and Goodrich C A. 2006. Nature and origins of meteoritic breccias. In: Meteorites and the Early Solar System II (Eds. Lauretta D S and McSween H Y Jr.), University of Arizona Press, Tucson. 679-712.

Bischoff A, Horstmann M, Barrat J-A, Chaussidon M, Pack A, Herwartz D, Ward D, Vollmer C and Decker S. 2014. Trachyandesitic volcanism in the early Solar System. PNAS 111, 12689-12692.

Bonin B. and Bébien J. 2005. The granite-upper mantle connection in terrestrial planetary bodies: an anomaly to the current granite paradigm? Lithos 80, 131-145.

Bonin B. 2012. Extra-terrestrial igneous granites and related rocks: A review of their occurrence and petrogenesis. Lithos 153, 3-24.

Bridges J C, Franchi I A, Hutchison R, Morse A D, Long J V P and Pillinger C T. 1995. Cristobalite- and tridymite-bearing clasts in Parnallee (LL3) and Farmington (L5). Meteoritics 30, 715-727.

Chaussidon M., Libourel G., Krot A.N. 2008. Oxygen isotopic constraints on the origin of magnesian chondrules and on the gaseous reservoirs in the early Solar System. Geochimica et Cosmochimica Acta 72, 1924-1938.

Clayton R. N. and Mayeda T. K. 1996. Oxygen isotope studies of achondrites. Geochimica et Cosmochimica Acta 60, 1999-2017.

Clayton R.N. and Mayeda T.K. 1988. Formation of ureilites by nebular processes. Geochimica et Cosmochimica Acta 52, 1313-1318.

Cohen B., Goodrich C.A. and Keil K. 2004. Feldspathic clast populations in polymict ureilites: Stalking the missing basalts from the ureilite parent body. Geochimica et Cosmochimica Acta 68, 4249-4266.

Day J.M.D., Ash R. D., Liu Y., Bellucci J. L., Rumble III D., McDonough W. F., Walker R. J. and Taylor L. A. 2009. Early formation of evolved asteroidal crust. Nature 457, 179-182.

Downes H., Mittlefehldt D.W., Kita N.T. and Valley J.W. 2008. Evidence from polymict ureilite meteorites for a disrupted and re-accreted single ureilite parent asteroid gardened by several distinct impactors. Geochimica et Cosmochimica Acta 72, 4825-4844.

Folco L., Franchi I.A., D'Orazio M., Rocchi, S. and Schultz L. 2000. A new Martian meteorite from the Sahara: The shergottite Dar al Gani 489. Meteoritics and Planetary Science 35, 827-839.

Goodrich C.A., Scott E.R.D. and Fioretti A.M. 2004. Ureilitic breccias: clues to the petrological structure and impact disruption of the ureilite parent asteroid. Chemie der Erde 64, 283-327.

Goodrich C. A., Bischoff A. and O'Brien D. P. 2014. Asteroid 2008 TC_3 and the fall of Almahata Sitta, a unique meteorite breccia. Elements 10, 31-37.

Goodrich C. A. and Gross J. 2015. A New Type of Ordinary Chondrite (?) Clast in Polymict Ureilite DaG 319. Lunar and Planetary Science Conference XXXXVI, Abst. 1241.

Gardner-Vandy K. G., McCoy T. J. and Bullock E. S. 2014. Making evolved melts on asteroids. Lunar and Planetary Science Conference XXXXV, Abst. 1483.

Gross J. and Filiberto, J. 2014a. Granitic compositions in gabbroic Martian meteorite NWA 6963 and a possible connection to felsic compositions on the Martian surface. Lunar and Planetary Science Conference XXXXV, Abst.1440~~–1441~~.

Gross J. and Filiberto, J. 2014b. Granitic compositions in gabbroic Martian meteorite NWA 6963: evidence for extreme fractional crystallization of a hydrous magma. Workshop on Volatiles in the Martian Interior. Lunar and Planetary Science Conference XXXXV, Abst. 1015.

Guan Y. and Crozaz G. 2000. Light rare earth element enrichments in ureilites: a detailed ion microprobe study. Meteoritics and Planetary Science 35, 131-144.

Guan Y. and Crozaz G. 2001. Microdistributions and petrogenetic implications of rare earth elements in polymict ureilites. Meteoritics and Planetary Science 36, 1039-1956.

Guitreau M, Blichert-Toft J, Martin H, Mojzsis S J, Albarede F. 2012. Hafnium isotope evidence from Archean granitic rocks for deep-manlte origin of continental crust. Earth Planet. Sci. Lett. 337-8, 211-223.

Hagerty J.J., Lawrence D.J., Hawke B.R., Vaniman D.T., Elphic R.C. and Feldman W.C. 2006. Refined thorium abundance for lunar red spots: Implications for evolved, nonmare

volcanism on the Moon. Journal of Geophysical Research, Planets 111. Online: E06002, doi:10.1029/2005JE002592.

Horstmann M. and Bischoff A. 2014. The Almahata Sitta polymict breccia and the late accretion of asteroid 2008 TC_3. Chemie der Erde 74, 149-183.

Ikeda Y. and Prinz M. 2001. Magmatic inclusions and felsic clasts in the Dar al Gani 319 polymict ureilite. Meteoritics and Planetary Science 36, 481-499.

Ikeda Y., Prinz M. and Nehru C.E. 2000. Lithic and mineral clasts in the Dar al Gani (DAG) 319 polymict ureilite. Antarctic Meteorite Research 13, 177-221.

Jolliff B.F., Floss C., McCallum I.S. and Schwartz J.M. 1990. Geochemistry, petrology, and cooling history of 14161,7373: A plutonic lunar sample with textural evidence of granitic-fraction separation by silicate-liquid immiscibility. American Mineralogist 44, 821-837.

Kita N.T., Ikeda Y., Togashi S., Liu Y., Morishita Y. and Weisberg M.K. 2004. Origin of ureilites inferred from a SIMS oxygen isotopic and trace element study of clasts in the Dar al Gani 319 polymict ureilite. Geochimica et Cosmochimica Acta 68, 4213-4235.

Kuehner S.M., Irving A.J., Korotev, R.L., Hupé G.M. and Ralew S. 2007. Zircon-baddeleyite-bearing silica + K-feldspar granophyric clasts in KREEP-rich lunar breccias Northwest Africa 4472 and 4485. Lunar and Planetary Science XXXVIII. 1516-1517.

Lambiv-Dzemua G., Gleeson S.A. and Schofield P.F. 2013. Mineralogical characterization of the Nkamouna Co-Mn laterite ore, southeast Cameroon. Minerallium Deposita 48, 155-171

Leshin L.A. and 33 co-authors,. 2013. Volatile, isotope, and organic analysis of Martian fines with the Mars Curiosity Rover. Science 341, 6153-6162.

Leroux H and Cordier P. 2006. Magmatic cristobalite and quartz in the NWA 856 Martian meteorite. Meteoritics and Planetary Science 41, 913-923.

Marinova M M, Aharonson O and Asphaug E. 2008. Mega-impact formation of the Mars hemispheric dichotomy. Nature 453, 1216-1219.

Martinez U.B. and Ryder G. 1989. A granite fragment from the Apennine Front - brother of QMD? Lunar and Planetary Science XX. 620-621.

Mittlefehldt D.W., McCoy T.J., Goodrich C.A. and Kracher A. 1998. Non-chondritic meteorites from asteroidal bodies. In: Planetary Materials. (Ed. J.J. Papike), Rev. Mineral. **36**, 4-1 - 4-195. Mineralogical Society of America, Washington, D.C.

Morris R.W., Taylor G.J., Newsom H.E. and Keil K. 1990. Highly evolved and ultramafic lithologies from the Apollo 14 soils. Proceedings 20th Lunar Scicence Conference. 61-75. Lunar and Planetary Institute, Houston.

Prinz M., Weisberg M.K., Nehru C.E., Delaney J.S. 1987. EET 83309, a polymict ureilite: recognition of a new group. Lunar and Planetary Science18, 802-803.

Rai V.K., Murthy A.V.S. and Ott U. 2003. Noble gases in ureilites: cosmogenic, radiogenic and trapped components. Geochimica et Cosmochimica Acta 67, 4435-4456.

Righter K, Collins S J and Brandon A D. 2005. Mineralogy and petrology of the LaPaz Icefield lunar mare basaltic meteorites. Meteoritics and Planetary Science 40, 1703-1722.

Rutherford M.J., Hess P.C., Ryerson F.J., Campbell H.W. and Dick P.A. 1976. The chemistry, origin and petrogenetic implications of lunar granite and monzonite. Proceedings 7th Lunar Science Conference, 1723-1740.

Ruzicka A., Hutson M. and Floss C. 2006. Petrology of silicate inclusions in the Sombrerete ungrouped iron meteorite: implications for the origins of IIE-type silicate-bearing irons. Meteoritics and Planetary Science, 41, 1797-1831.

Ruzicka A. and Hutson M. 2010. Comparative petrology of silicates in the Udei Station (IAB) and Miles (IIE) iron meteorites: Implications for the origin of silicate-bearing irons. Geochimica et Cosmochimica Acta 74, 394-433.

Ruzicka A. 2014. Silicate-bearing iron meteorites and their implications for the evolution of asteroidal parent bodies. Chemie der Erde 74, 3-48.

Ryder G. 1976. Lunar sample 15405: Remnant of a KREEP basalt-granite differentiated pluton. Earth and Planetary Science Letters 29, 255-268.

Sokol A. K., Chaussidon M., Bischoff A. and Mezger K. 2007. Occurrence and origin of igneous fragments in chondritic breccias. V M Goldschmidt Conference, Abstract A952

Streckeisen A. 1976. To each plutonic rock its proper name. Earth Science Reviews 12, 1-33.

Takeda H., Hsu W. and Huss G. R. 2003. Mineralogy of silicate inclusions of the Colomera IIE iron and crystallization of Cr-diopside and alkali feldspar from a partial melt. Geochimica et Cosmochimica Acta 67, 2269-2288.

Terada K. and Bischoff A. 2009. Asteroidal granite-like magmatism 4.53 Gyr ago. The Astrophysical Journal 699, L68-L71.

Usui T., Jones J H and Mittlefehldt D W. 2015. A partial melting study of an ordinary (H) chondrites composition with application to the unique achondrite Graves Nunataks 06128 and 06129. Meteoritics and Planetary Science. Online: doi: 10.1111/maps.12392

Varela M. E., Kurat G., Bonnin-Mosbah M., Clocchiatti R. and Massare D. 2000. Glass-bearing inclusions in olivine of the Chassigny achondrite: Heterogeneous trapping at sub-igneous temperatures. Meteoritics and Planetary Science 35, 39-52.

Warren P., Taylor G. J., Keil K., Shirley D. N. and Wason, J. T. 1983. Petrology and chemistry of two "large" granite clasts from the Moon. Earth and Planetary Science Letters, 64, 175-185.

Warren P. and Kallemeyn G. W. 1989. Geochemistry of polymict ureilite EET83309, and a partially-disruptive impact model for ureilite origin. Meteoritics 24, 233-246.

Wedepohl K. H. 1991. Chemical composition and fractionation of the continental crust. Geologishe Rundschau 80, 207-223.

Wittmann A., Korotev R. L., Jolliff B. L., Irving A. J., Moser D.E., Barker I., and Rumble D. 2015. Petrography and composition of Martian regolith breccia meteorite Northwest Africa 7475. Meteoritics and Planetary Science 50, 326-352.

Young E. D. and Russell S. S. 1998. Oxygen reservoirs in the early solar nebula inferred from an Allende CAI. Science 282, 452-455.

Figure Captions

Figure 1. BSE image of EET 87720,41 showing location of the microgranitic clast. The clast can be clearly separated from the enclosing ureilitic material, but different phases within the clast cannot be distinguished.

Figure 2. Elemental distribution maps of Si, Al, Na, K, Ca within the microgranitic clast in EET 87720,41, showing the granophyre-like intergrowth and the zoned oligoclase sharing a common margin. Colours indicate relative intensity of elemental concentrations

(i.e. reds, pinks = high concentrations; greens = medium concentrations; blues = low concentrations). Oligoclase phenocryst is the rectangular object on the right-hand side (clearly shown on Si, Na and Al images); zonation from core to rim is shown in Ca image. Top right image BSE image of the clast shows that its constituent phases all have very similar low mean atomic numbers.

Figure 3. Ab-An-Or ternary diagram showing the plagioclase composition for the microgranitic clast in EET 87720,41. Feldspar compositions from the granitic clasts in the LL3-6 chondritic breccia Adzhi-Bogdo (Bischoff et al., 1993), lunar granite samples (Ryder, 1976; Warren et al., 1983; Jolliff et al., 1990), feldspathic clasts from polymict ureilite DaG 319 (Ikeda and Prinz, 2001, Ikeda et al, 2000), and mean plagioclase compositions in silicate inclusions in iron meteorites (Ruzicka, 2014) have been plotted for comparison.

Figure 4. Total Alkali vs Silica diagram showing estimated bulk chemical composition of microgranitic clast in EET 87720,41, compared with compositions of glassy inclusions in IIE irons Colomera, Sombrerete and Weekeroo Station (Takeda et al. 2003; Ruzicka et al. 2006) and in granitic inclusions in Martian meteorite NWA 6963 (Gross and Filiberto, 2014a,b).

Figure 5. QAP diagram (Streckeisen, 1976) showing the microgranitic clast in EET 87720,41 plotting in the alkali granite field. Granitic clasts in the LL3-6 chondritic breccia Adzhi-Bogdo (Bischoff et al., 1993), silica-rich glass inclusions in polymict ureilite DaG 319 (Ikeda and Prinz, 2001, Ikeda et al, 2000), silica-rich glass inclusions in the Colomera IIE iron (Takeda et al., 2003), lunar granites (Warren et al., 1983; Ryder, 1976), felsic glass spherule in howardite NWA 1664 (Barrat et al., 2009) and selected silica-rich glass inclusions in olivine from Martian meteorites DaG 489 (Folco et al., 2000) and Chassigny (Varela et al., 2000) have been plotted for comparison.

Figure 6. Three isotopes of oxygen plot showing mean values for microgranite clast in EET87720,41 (Table 4), mean values for three granitic clasts in Adzhi-Bogdo (Sokol et

al., 2007), bulk ureilites (Clayton and Mayeda 1988), field for ordinary chondrites, silicate inclusions in IIE and IVAB iron meteorites, field for Martian meteorites (Clayton and Mayeda 1996), field for Mars breccia meteorites NWA 7034 (Agee et al., 2013) and NWA 7475 (Wittmann et al., 2015), GRA 06128/9 = andesitic meteorites (Day et al. 2009); TFL = Terrestrial Fractionation Line; CCAM = carbonaceous chondrites anhydrous mineral line; Young and Russell slope 1 line (Young and Russell, 1998).

Table captions

Table 1. Electron microprobe data for constituent minerals and glass in the microgranitic clast in EET 87720,41.

Table 2. Estimated modal proportions for the microgranitic clast in EET 87720,41, compared with other known extra-terrestrial granitic clasts.

Table 3. Calculated bulk rock and CIPW compositions for the microgranitic clast in EET 87720, 41, using the mineral compositions in Table 1 and modal proportions in Table 2. Glass (Table 1) was not included in the calculations.

Table 4. Oxygen isotope data for feldspars and tridymite in microgranitic clast within EET 87720,41, analysed by SIMS (CNRS-CRPG, Nancy, France).

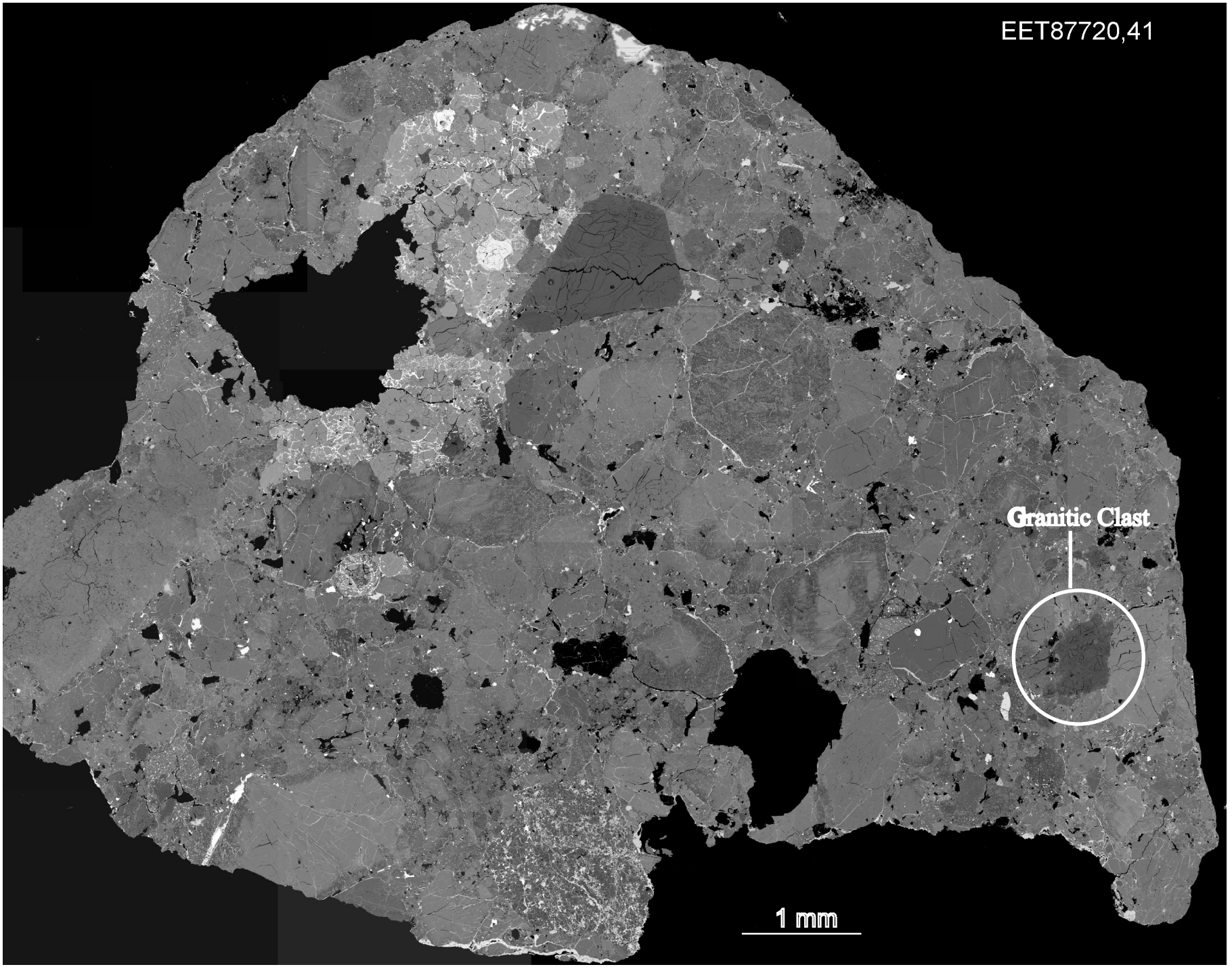
EET87720,41
Granitic Clast
1 mm

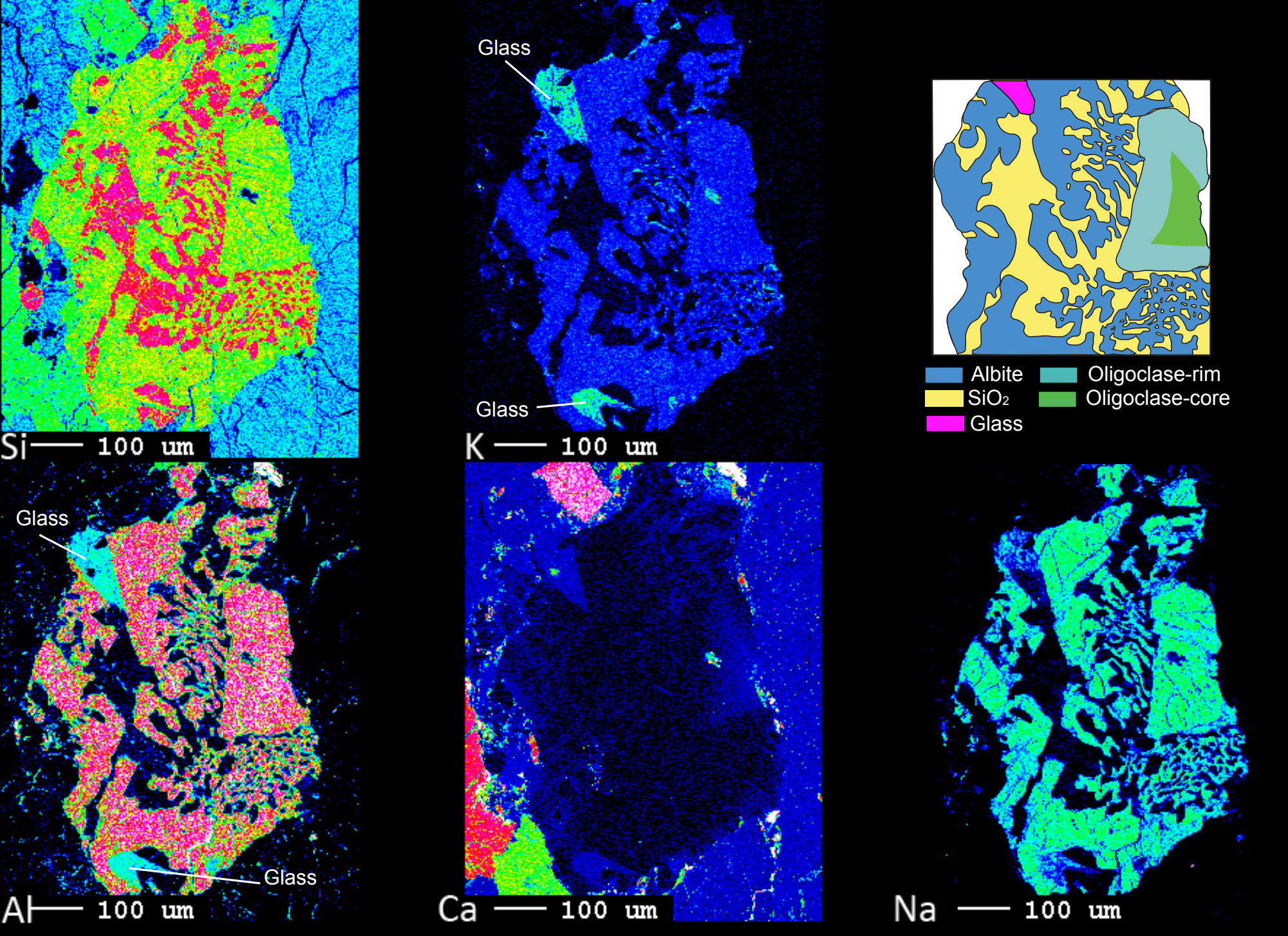
Glass
Glass
Glass
Glass
Albite
Oligoclase-rim
SiO2
Oligoclase-core
Glass
Si 100 um
K 100 um
Al 100 um
Ca 100 um
Na 100 um

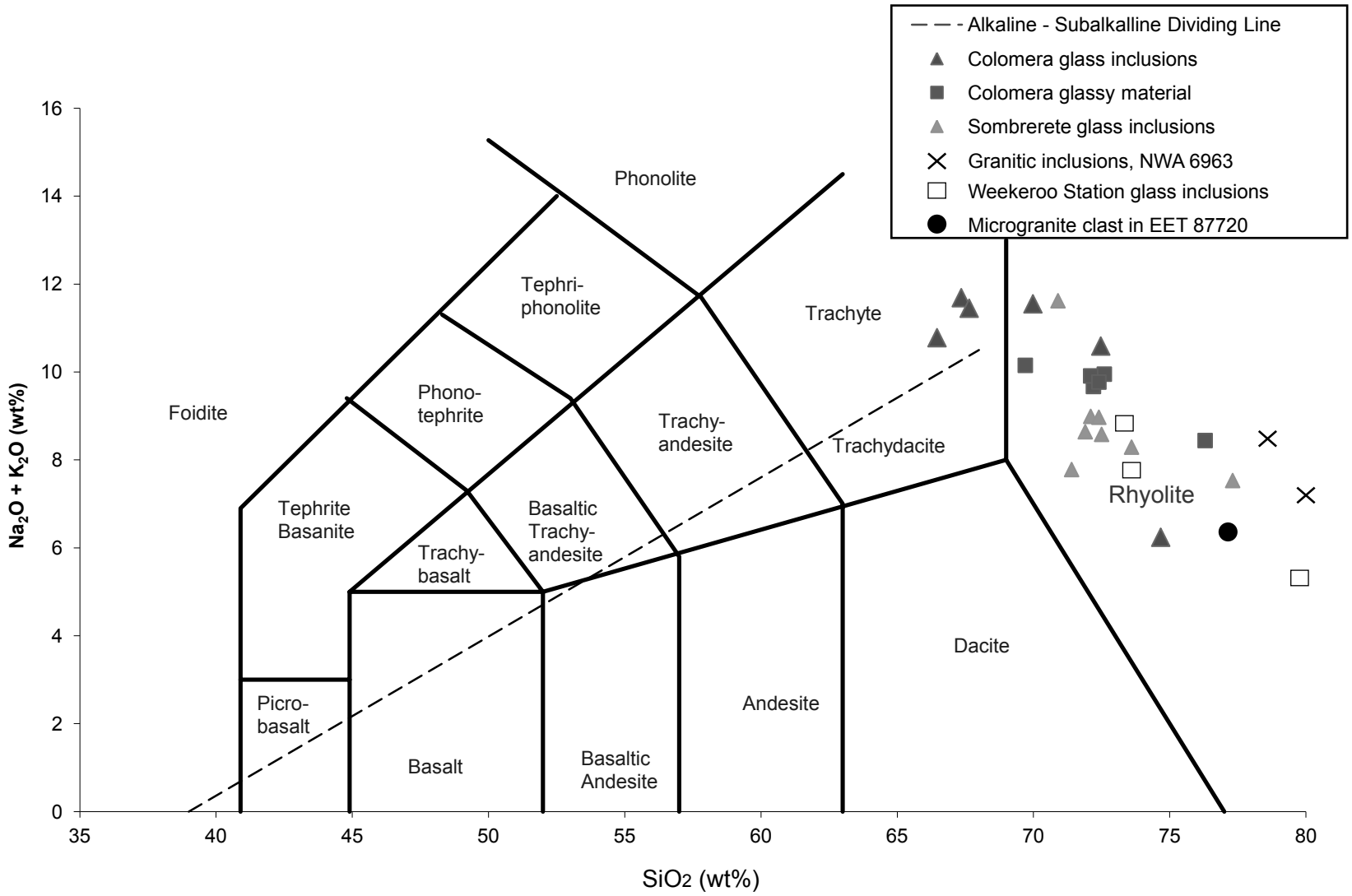
Alkaline - Subalkalline Dividing Line
Colomera glass inclusions
Colomera glassy material
Sombrerete glass inclusions
Granitic inclusions, NWA 6963
Weekeroo Station glass inclusions
Microgranite clast in EET 87720
Phonolite
Tephri-phonolite
Trachyte
Foidite
Phono-tephrite
Trachy-andesite
Trachydacite
Rhyolite
Tephrite Basanite
Basaltic Trachy-andesite
Trachy-basalt
Dacite
Picro-basalt
Andesite
Basalt
Basaltic Andesite
Na2O + K2O (wt%)
SiO2 (wt%)
0
2
4
6
8
10
12
14
16
35
40
45
50
55
60
65
70
75
80

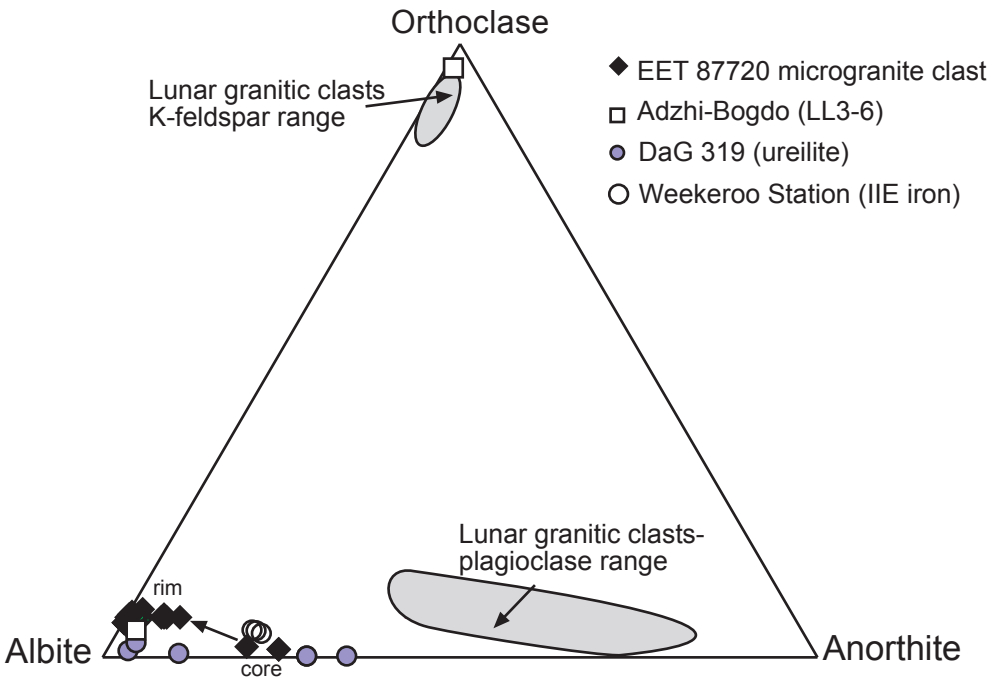
Orthoclase
Albite
Anorthite
Lunar granitic clasts
K-feldspar range
Lunar granitic clasts-
plagioclase range
rim
core
EET 87720 microgranite clast
Adzhi-Bogdo (LL3-6)
DaG 319 (ureilite)
Weekeroo Station (IIE iron)

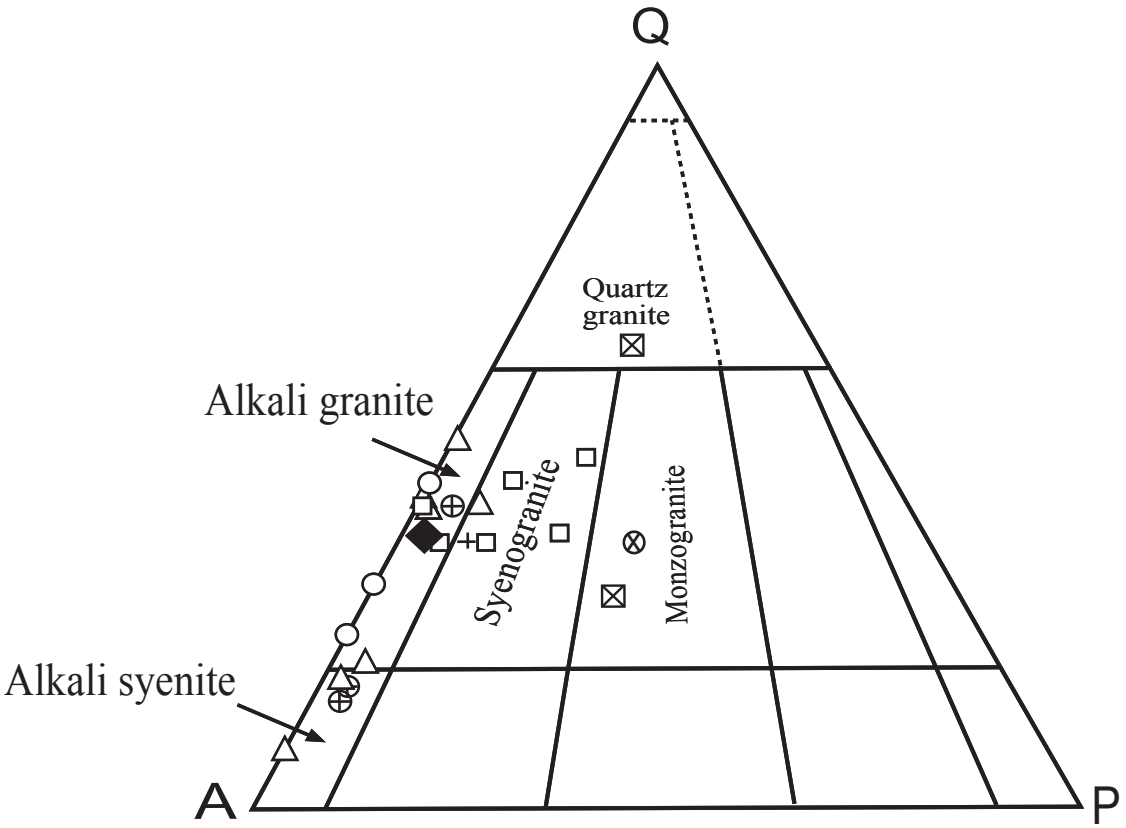

◆ Microgranite clast, EET 87720

△ DaG 319 (ureilite)

□ Lunar granites

○ Adzhi-Bogdo (LL3-6)

⊠ DaG 489 (shergottite)

⊕ Colomera IIe iron meteorite

\+ Chassigny

⊗ Felsic glass spherule, NWA 1664 (howardite)

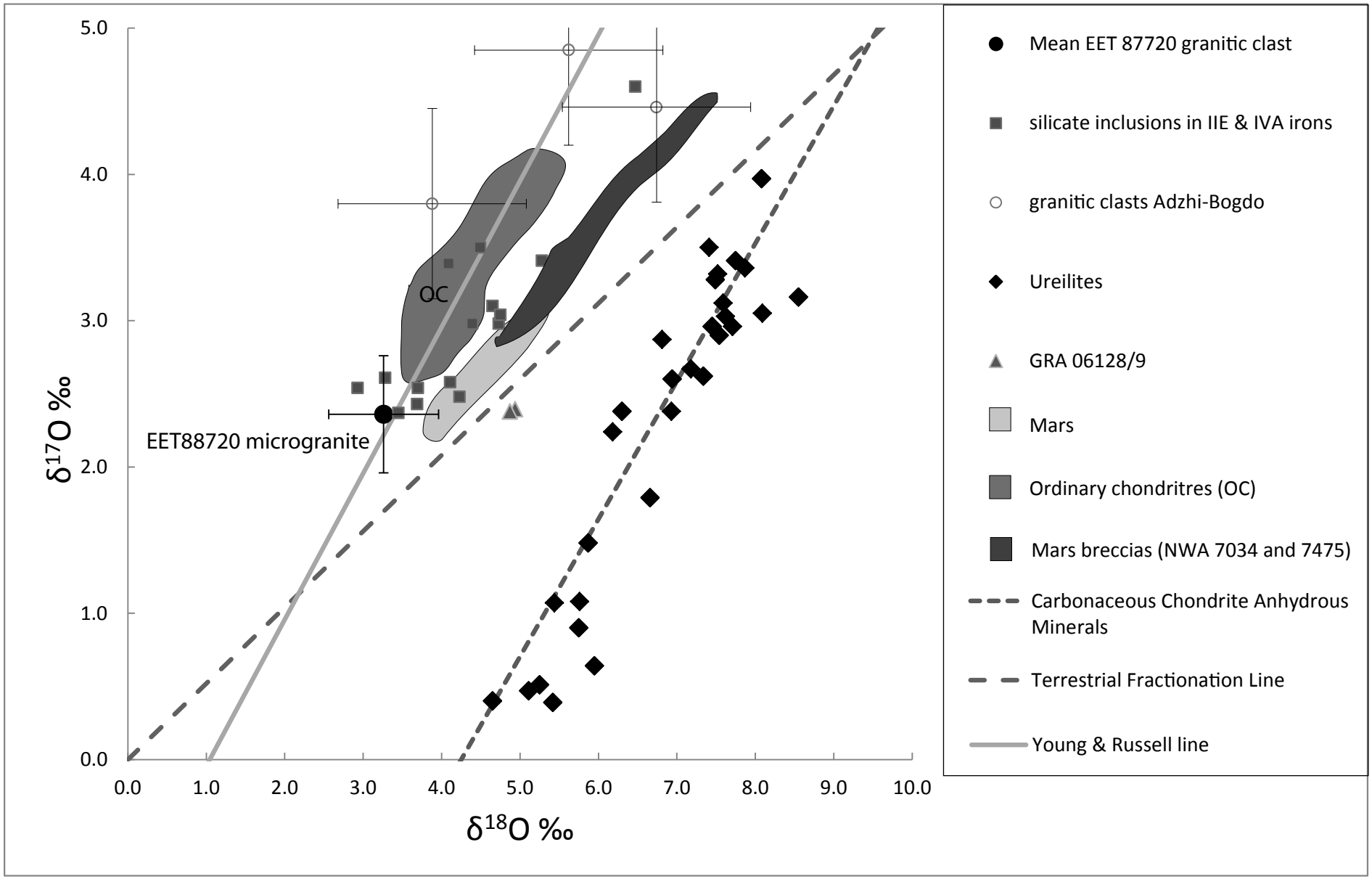
5.0
4.0
3.0
2.0
1.0
0.0
0.0
1.0
2.0
3.0
4.0
5.0
6.0
7.0
8.0
9.0
10.0
δ17O ‰
δ18O ‰
OC
EET88720 microgranite
Mean EET 87720 granitic clast
silicate inclusions in IIE & IVA irons
granitic clasts Adzhi-Bogdo
Ureilites
GRA 06128/9
Mars
Ordinary chondritres (OC)
Mars breccias (NWA 7034 and 7475)
Carbonaceous Chondrite Anhydrous Minerals
Terrestrial Fractionation Line
Young & Russell line

Table 1. Electron microprobe data for constituent minerals and glass in the microgranitic clast in EET 87720,41

	Granophyre-like intergrowth		Oligoclase				
			core	rim 1	rim 2		Glass phase
	Silica phase	Albite					
SiO_2	98.19	69.60	63.81	68.16	69.81	SiO_2	72.51
TiO_2	0	0	0	0	0	TiO_2	0.06
Al_2O_3	1.16	17.93	21.71	17.75	18.37	Al_2O_3	9.36
FeO	0.12	0.10	0.94	0.51	0.15	FeO	0.95
MnO	0.01	0	0	0	0	MnO	0.01
CaO	0	0.84	4.89	0.03	0.02	Cr_2O_3	0.01
MgO	0.02	0	0	0	0	NiO	0.13
Na_2O	0.12	10.09	8.48	10.33	11.02	CaO	0.42
K_2O	0.08	1.10	0.25	0.97	1.02	MgO	2.84
						Na_2O	0.39
Total	99.70	99.67	100.08	97.75	100.39	K_2O	1.18
						SO_3	11.36
	An	1.93	12.29	0.07	0.05	Cl	0.60
	Ab	92.12	86.22	97.12	99.26		
	Or	5.92	1.49	2.81	0.79	Total	99.81

Table 2. Estimated modal proportions for the microgranite clast in EET 87720,41, compared with other known extraterrestrial granitic clasts.

	EET 87720,41 Polymict ureilite	Lunar Apollo 14 breccia 14321	Lunar Apollo 14 breccia 14321	Adzhi-Bogdo Chrondrite (LL3-6) Clast A	Adzhi-Bogdo Chrondrite (LL3-6) Clast B	Adzhi-Bogdo Chrondrite (LL3-6) Clast C	Adzhi-Bogdo Chrondrite (LL3-6) Clast D
%							
Quartz	30	40	23	22.9	26	43.7	30
K-feldspar		60 (Or_{89})	32(Or_{93})	58.9($Or_{96.1}$)	35($Or_{96.4}$)	55.9($Or_{96.2}$)	68.8($Or_{97.3}$)
Albite	55 (Ab_{99})		33 (An_{86-59})	15.8($Ab_{93.7}$)			
Plagioclase	15 (An_{12})						
Clinopyroxene		trace	11	1.3	1.6		
Ilmenite		trace	1	0.8	21.7	<0.1	0.1
Comments and accessory phases	granophyre-like intergrowth	graphic texture (qtz-K-feld intergrowth)	graphic texture (qtz-K-feld intergrowth)	Apatite Zircon	Apatite Whitlockite Zircon	Zircon	Apatite Zircon

Table 3. Calculated bulk rock and CIPW compositions for the microgranitic clast in EET 87720, 41, using the mineral compositions in Table 1 and modal proportions in Table 2. Glass (Table 1) was not included in the calculations.

		CIPW Norm	
SiO_2	77.31	Quartz (Q)	32.91
Al_2O_3	13.47	Orthoclase (Or)	3.96
FeO	0.23	Albite (Ab)	58.05
CaO	1.20	Anorthite (An)	3.98
Na_2O	6.86	Diopside (Di)	0.79
K_2O	0.67	Wollastonite (Wo)	0.45
Total	99.73	Total	100.14

Table 4. Oxygen isotope data for feldspars and tridymite in microgranitic clast within EET 87720,41, analysed by SIMS (CNRS-CRPG, Nancy, France).

	$\delta^{18}O‰$	±2σ	$\delta^{17}O‰$	±2σ	$\Delta^{17}O‰$	±2σ
Point 1	3.92	0.51	2.72	0.66	0.68	0.60
Point 2	2.59	0.56	1.78	0.61	0.43	0.56
Point 3	1.95	0.52	1.45	0.76	0.44	0.70
Point 4	3.93	0.53	2.44	0.73	0.40	0.67
Point 5	3.85	0.55	2.58	0.78	0.58	0.73
Point 7	3.66	0.51	2.49	0.70	0.59	0.64
Point 8	2.72	0.55	2.56	0.74	1.15	0.69
Point 9	3.69	0.53	2.87	0.70	0.95	0.64
Point 10	0.32	0.50	2.13	0.64	0.47	0.57
Point 11	3.14	0.54	2.55	0.77	0.92	0.72
Mean	3.26		2.36		0.66	
±2σ	1.34		0.88		0.52	